Rotating Fluidized Beds in a Static Geometry: Experimental Proof of Concept

Juray De Wilde and Axel de Broqueville
Dept. of Materials and Process Engineering (IMAP), Université Catholique de Louvain, B-1348 Louvain-la-Neuve, Belgium

DOI 10.1002/aic.11139
Published online March 2, 2007 in Wiley InterScience (www.interscience.wiley.com).

The new concept of a rotating fluidized bed in a static geometry (RFB-SG) is presented. The rotating motion of the particle bed and the tangential fluidization of the solids are obtained by the tangential injection of the fluidization gas via multiple gas inlet slots in the outer cylindrical wall of the fluidization chamber. The solids experience a radially outwards centrifugal force. The gas, on the other hand, is forced to move radially inwards towards a chimney with one or more outlet slots, creating a radially inwards gas-solid drag force and fluidizing the solids radially. The new fluidization concept is experimentally investigated and proven using one and the same non-optimized fluidization chamber design with either large diameter, low density polymer particles or small diameter, higher density Alumina particles. The fluidization chamber is operated in continuous mode, at different solids loadings and in the vertical and horizontal position. © 2007 American Institute of Chemical Engineers *AIChE J,* 53: 793–810, 2007

Keywords: fluidization, rotating fluidized bed, centrifugal force, reactors, gas-solid flow

Introduction

In so-called rotating fluidized beds (RFB), a radially outwards centrifugal force exerted on the solids is balanced by a radially inwards gas-solid drag force. The latter result from a radially inwards moving fluidization gas. Because of the centrifugal force, the rotating fluidized bed has a cylindrical shape. RFB have flow characteristics that are advantageous over those of conventional (i.e. gravitational) fluidized beds for a variety of applications.[1,2] In fact, almost any advantage of the conventional fluidized beds is maintained or increased.

The centrifugal force is determined by the rotational speed of the particle bed and can be a multiple of earth gravity, allowing a vertical or horizontal operation, much higher fluidization gas velocities and increased (radial) gas-solid slip velocities. The latter is expected to significantly improve the inter-phase mass and heat transfer. Therefore, RFB are potentially advantageous for use with exothermic/endothermic reactions[2] or for drying applications. Because of the centrifugal force, excellent gas-solid separation can be obtained,[3] despite higher fluidization gas velocities. High rotational speeds are reported to allow more gas throughput without serious formation of bubbles or a slugging bed.[2] This allows for example to increase the efficiency and improve the flexibility of gas phase polymerization reactors.[2] The cylindrical shape of the rotating fluidized bed allows a very high ratio between its freeboard surface and its thickness (height in conventional fluidized beds) and a more compact construction.

RFB have attracted special interest recently, because of their advantages in fluidizing very fine particles, such as cohesive (Geldart group C), micro-, and nano-particles.[1,4–7] In fact, it has been shown that such particles can be uniformly fluidized in a centrifugal force field that is sufficiently strong to overcome the interparticle van der Waals forces.[4,7,8] The

Correspondence concerning this article should be addressed to J. De Wilde at dewilde@imap.ucl.ac.be.

strong centrifugal force allows an increased gas throughput without entrainment of particles.[9] RFB have been used for fluidizing, granulating, and coating fine powders to tailor their properties and functionalities.[5,6]

The centrifugal force requires a rotating motion. In the RFB investigated so far (named conventional RFB in what follows),[1–15] a motor is used to rotate the reactor or fluidization chamber fast around its axis of symmetry. The fluidization gas is radially introduced in the fluidization chamber by means of gas distributors in the rotating outer cylindrical wall of the fluidization chamber. Usually a porous or sintered wall is used.[1,3–5,10,11] Slotted gas distributors have been studied as well.[10] Obvious disadvantages of the conventional rotating fluidized bed technology are the use of a motor and the moving geometry, i.e. the rotating fluidization chamber. The latter may, for example, be at the origin of mechanical vibrations or complicate sealing, the feeding or removal of the solids to/from the fluidization chamber and continuous operation. Therefore, experiments with conventional RFB commonly start with a batch of particles being loaded into the fluidization chamber.[4,5,10]

To overcome the difficulties related to a rotating geometry, the new concept of a rotating fluidized bed in a static geometry (RFB-SG) is proposed and investigated. First, the new concept is described. Next, experimental proof of concept is given. Using one and the same nonoptimized fluidization chamber geometry, the fluidization of two types of particles is studied at different solids loadings and in the vertical and horizontal operation.

The Concept of a Rotating Fluidized Bed in a Static Geometry

To induce a rotating motion in the static geometry, the fluidization gas is injected tangentially via multiple gas inlet slots at the outer cylindrical wall of the fluidization chamber (Figure 1a).[16] As a result of the tangential gas-solid drag force, the solid particles in the fluidization chamber rotate as well and experience a radially outwards centrifugal force. By the action of the centrifugal force, the particles tend to form a rotating particle bed against the outer cylindrical wall of the fluidization chamber. On average, the tangential gas-solid slip velocity is expected to be small ($v_t = u_t$), in contrast to the radial gas-solid slip velocity. Locally, however, in particular in the vicinity of the gas inlet slots, the tangential gas-solid slip velocity can be very large, depending on the difference between the gas injection velocity and the particle bed rotational speed. The gas is moving radially inwards (Figure 1b), forced to leave the fluidization chamber via an inner chimney with one or multiple outlet slots (Figure 1a). The solids experience a radially inwards gas-solid drag force counteracting the radially outwards centrifugal force. The relative importance of the two forces depends on the operating conditions and on the fluidization chamber design, in particular its outer and inner (chimney) diameter, its length, and the number of gas inlets, their surface area, and eventually their angle of injection. A proper fluidization chamber design allows to balance the centrifugal force and the drag force (Figures 1a,b) and the radial fluidization of the rotating particle bed. It should be remarked that with respect to the centrifugal force, the behavior of the RFB-SG has similarities with the behavior observed in cyclones.

Assuming that in the particle bed the particles are radially fluidized and the radial motion of the particles is negligible,

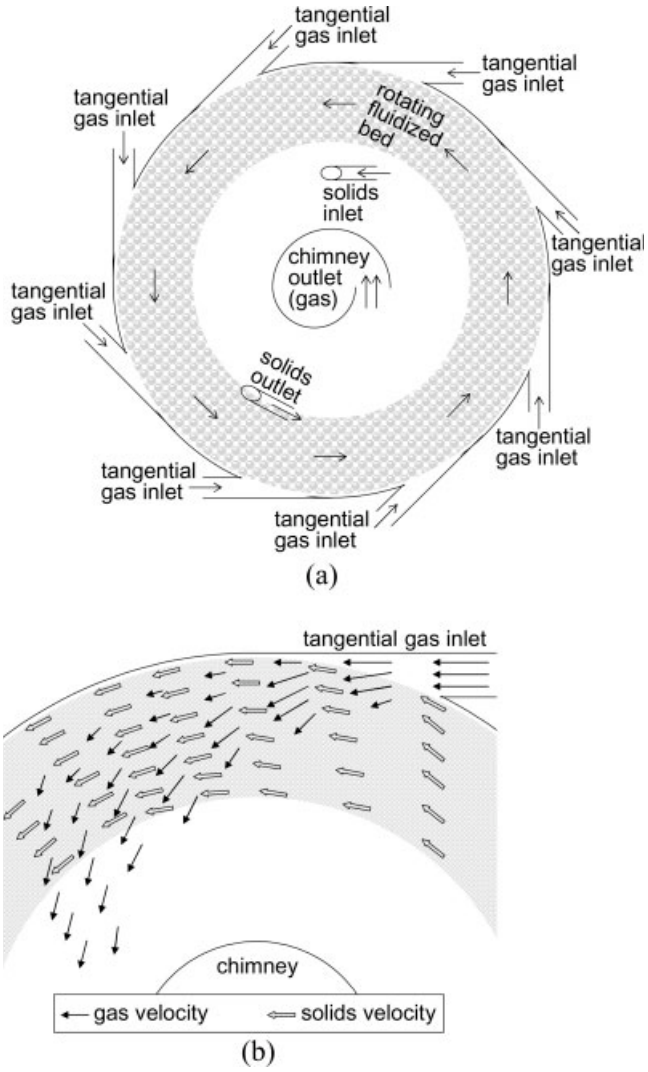

Figure 1. Representation of the concept of a RFB-SG.

(a) 2D section of the fluidization chamber; (b) detail of the gas and solids velocity behavior near a tangential gas inlet of the fluidization chamber.

the radially inwards gas-solid drag force is given by[17,18]:

$$\beta(u_r - v_r) \approx \beta u_r \tag{1}$$

with the drag coefficient β for example given by:

$$\beta = 150\frac{\varepsilon_s^2}{\varepsilon_g}\frac{\mu_g}{(d_p\phi)^2} + 1.75\frac{\varepsilon_s\rho_g}{d_p\phi}|\bar{u} - \bar{v}| \quad \text{for} \quad \varepsilon_g < 0.80 \tag{2}$$

$$\beta = \frac{3}{4}C_{d,s}\frac{\varepsilon_g\varepsilon_s}{d_p\phi}\rho_g|\bar{u} - \bar{v}|\varepsilon_g^{-2.65} \quad \text{for} \quad \varepsilon_g \geq 0.80 \tag{3}$$

and:

$$C_{d,s} = \frac{24}{Re_p}(1 + 0.15Re_p^{0.687}) \quad \text{if} \quad Re_p \leq 1000 \tag{4}$$

$$C_{d,s} = 0.44 \quad \text{if} \quad Re_p > 1000 \tag{5}$$

the particle Reynolds number Re_p being defined as:

$$Re_p = \frac{|\bar{u} - \bar{v}|\varepsilon_g \rho_g d_p \phi}{\mu_g} \quad (6)$$

If the solids volume fraction is below 0.2 and the particle Reynolds number Re_p is sufficiently high, the radially inwards gas-solid drag force is roughly proportional to the square of the radial (interstitial) gas velocity.[17] In case the solids volume fraction is higher than 0.2 and/or the particle Reynolds number is sufficiently low or in case the particles are radially not fluidized, forming a sort of rotating packed particle bed, the radially inwards gas-solid drag force is roughly proportional to the radial gas velocity u_r,[18] rather than to its square. The tangentially averaged radial gas velocity, which roughly equals the radial gas-solid slip velocity, can be calculated from:

$$u_r = \frac{F_g}{2\pi r L \varepsilon_g} \quad (7)$$

and depends logically on the total gas flow rate F_g, the fluidization chamber length L, the radial position r (Figure 1) and the local void fraction ε_g.

Assuming on average a solid body rotation of the particle bed, the radially outwards centrifugal particle acceleration could be calculated from:

$$a_r = \omega^2 r = \frac{v_t^2}{r} \quad (8)$$

Deviations from the solid body rotation motion of the particle bed are expected to occur locally as a result of particle-wall collisions and the related shear and as a result of the periodical tangential gas injection, so in particular in the vicinity of the gas inlet slots. Right upstream of a gas inlet slot, the tangential motion of the particle bed is expected to slow down and some particle accumulation is expected to occur. In front of a gas inlet, on the other hand, the particle bed is expected to be tangentially accelerated. Hence, it is expected that in practice, a dynamic component must be added to the average motion of the particle bed. The relative importance of this dynamic component is expected to depend on the type of particles that are fluidized. This is to be further investigated.

Kroger et al.[12] showed in a conventional rotating fluidized bed that for large size particles (larger than about 500 μm) at initial fluidization, the fluidized bed rotates indeed like a solid body ($v_t = \omega r$) because of the large effective viscosity. The effective viscosity decreasing strongly with decreasing particle size and increasing bed porosity, small (micro, nano) size particles characterized by a significant bed expansion result in a small effective viscosity and a tangential velocity profile similar to a free vortex ($v_t = Cr_{distr}/r$).

Simulations of the gas flow through and in a particle free rotating cylinder of a conventional rotating fluidized bed[6] showed that the gas velocity is mostly tangential and vortex like, the gas flow far from being solid body like. The gas flow pattern is, however, expected to be strongly affected by the presence of a particle bed.[2] In RFB-SG, the gas phase motion is certainly not solid body rotation like. As shown in Figure 1, the gas enters periodically through the tangential gas inlet slots. Immediately after injection through a gas inlet slot, the gas is squeezed between the outer cylindrical wall of the fluidization chamber and the rotating particle bed. Next, the gas crosses the particle bed in a combined rotational/radial motion. The gas injected via a given gas inlet slot is expected to have crossed the particle bed before new gas is injected via the next gas inlet slot. Once in the gas zone near the chimney, the gas is directed in another and different combined rotational/radial motion towards the outlet(s) to the chimney.

As in conventional RFB, the variation of the drag force and the centrifugal force with the radial position should result in layered fluidization.[8,13,14] In conventional RFB, with increasing radial gas velocity, the particle bed changes from a packed bed to a partially fluidized bed and further to an entirely fluidized bed, the fluidization starting at the inner surface of the particle bed because there the drag force is highest and the centrifugal force is lowest.[11] As such, the surface minimum fluidization velocity, the critical fluidization velocity—that is when the particles at the gas distributor are fluidized—and the average fluidization velocity can be distinguished between.[10,14]

For a given total gas flow rate F_g and outer fluidization chamber diameter, the tangential velocity in the fluidization chamber and, hence, the centrifugal force Eq. 8 can be increased by decreasing the fluidization chamber volume. The latter can be achieved by increasing the inner fluidization chamber diameter, that is, the chimney diameter.

For a given fluidization chamber volume V and total gas flow rate F_g, and assuming the gas residence time to be given by (V/F_g), the particle bed thickness to be small when compared with the outer fluidization chamber radius R, and a uniform dense particle bed at sufficiently low particle Reynolds number, the ratio of the centrifugal force and the gas-solid drag force can, for example, be increased by increasing the outer (R) and inner (chimney) radius of the fluidization chamber, keeping its length (L) fixed. Indeed, according to Eqs. 1–7, the gas-solid drag force decreases roughly inversely proportional to the outer fluidization chamber radius, whereas according to Eq. 8, the centrifugal force increases roughly proportional to the outer fluidization chamber radius. In case the fluidization chamber length (L) would be decreased to keep the fluidization chamber volume (V) fixed when increasing the outer fluidization chamber radius (R) while keeping the inner (chimney) radius fixed, the ratio of the centrifugal force and the gas-solid drag force would be hardly affected. Indeed, the outer fluidization chamber radius (R) being much larger than the inner (chimney) fluidization chamber radius, the fluidization chamber length (L) has to be roughly reduced inversely proportional to the square of the outer fluidization chamber radius. In such case ($L \sim R^{-2}$), according to Eqs. 1–8, both the gas-solid drag force and the centrifugal force increase roughly proportional with the outer fluidization chamber radius.

Keeping the outer (R) and inner (chimney) radius as well as the length (L) of the fluidization chamber fixed, the ratio of the centrifugal force and the gas-solid drag force can be altered by adapting the design of the gas inlet slots, as explained hereafter.

For a given total gas flow rate

$$F_g = n_g^{in} S_g^{in} u_g^{in} \tag{9}$$

the tangential momentum introduced in the fluidization chamber

$$M_t^{in} = n_g^{in} S_g^{in} \rho_g^{in} u_g^{in} u_g^{in} \tag{10}$$

can be optimized via the number of gas inlets n_g^{in} and their surface area S_g^{in}. Reducing the number of gas inlets n_g^{in} or their surface area S_g^{in} increases the tangential momentum injected for a given gas flow rate F_g. The uniformity of the gas distribution over the particle bed should, however, also be accounted for in view of the local radially inwards gas motion required for the radial fluidization. Hence, optimum values for the number of gas inlets and the gas inlet surface area exist.

It should be remarked that the use of slotted gas distributors in conventional RFB resulted in nonuniform fluidization and restructuring of the fluidized bed, the fluidization occurring primarily over the slots.[10] In the new RFB-SG, the nonuniformity introduced by slotted gas distributors is much less pronounced because of the tangential distribution of the gas over the fluidized bed. However, in future work, more complex sintered tangential gas distributors may be investigated.

The optimal fluidization chamber design depends on the properties of the particles to be fluidized. For a given fluidization chamber geometry, optimized for a given type of particles, increasing the gas flow rate F_g increases the tangential velocity in the fluidization chamber u_t and the resulting centrifugal force Eq. 8 (roughly $\sim u_t^2$), on the one hand, and the radial velocity in the fluidization chamber u_r and the resulting radial gas-solid drag force Eq. 1 (roughly (u_r or $\sim u_r^2$, depending on the conditions), on the other hand. Hence, for the given fluidization chamber geometry for the given type of particles and for rotational speeds sufficiently high to allow neglecting gravity and conditions that allow to approach a dependence to the square of the radial gas velocity of the radial gas-solid drag force, it should be possible to balance the centrifugal force and the radial gas-solid drag force over a relatively broad gas flow rate range. This is an important advantage of RFB-SG. For the experimental proof of concept in what follows, one and the same nonoptimized fluidization chamber geometry is used with different particles.

The average gas phase pressure drop over the fluidization chamber is determined by: (a) the "weight" of the particle bed in the centrifugal field ($\approx \rho_s(1-\varepsilon_g)r\omega^2$) related to the radial fluidization of the particle bed, (b) the shear within the gas phase, and (c) the gas-solid momentum transfer to create the rotational motion of the particle bed in the static geometry and to compensate for particle-wall interactions. The local gas phase pressure gradients differ, however, considerably throughout the rotating particle bed, in particular with the tangential position in the fluidization chamber. Immediately upstream of each gas inlet, gas velocities are low compared to the gas inlet velocity and the radial fluidization of the particle bed is expected to be minimal whereas the hydrostatic gas phase pressure is expected to be relatively high. Immediately in front of each gas inlet, on the other hand, the gas velocity should be high compared to the average gas velocity in the fluidization chamber to inject sufficient tangential momentum (Eq. 10) and the radial fluidization of the particle bed is expected to be the most pronounced, resulting in relatively low hydrostatic gas phase pressures. Hence, because of the periodical injection of gas in the fluidization chamber, the gas phase pressure exerted on the rotating particles contains a dynamic component, that is, increases and decreases periodically with the tangential position in the fluidization chamber. The relative importance of the dynamic component depends on the type of particles being fluidized and the operating conditions.

The momentum and energy needs are periodically provided via the gas inlets. Because of the tangential fluidization (beside the radial fluidization) and the relation between the gas velocity and the particle bed rotational speed in RFB-SG, the relation between the gas phase pressure drop over the fluidization chamber and the gas velocity is more complex for RFB-SG than for conventional (rotating) fluidized beds.

It should be emphasized that the gas injected in the fluidization chamber exerts both a tangential and a radial force on the particles. As such, the gas injected serves both as the driving power for the rotational motion in the fluidization chamber and as fluidization gas. The tangential and radial motion of the gas in the fluidization chamber implies, however, a combined tangential and radial fluidization of the particle bed. Whereas in the radial direction, the centrifugal force is to be balanced by the radial drag force, in the tangential direction, the tangential drag force is used to create the rotational motion of the particle bed and to counteract the shear stress mainly due to particle-wall collisions.

The RFB-SG may find applications similar to those of the conventional RFB which are discussed in the Introduction and references.[1–6] Furthermore, whereas the advantages of the conventional rotating fluidized bed are maintained, its disadvantages related to the use of a motor and the rotating geometry are eliminated. In particular, the static geometry reduces mechanical vibrations, eliminates the need for a rotating seal, and facilitates the feeding and removal of particles to/from the fluidization chamber, the control of the solids hold-up and continuous operation. The RFB-SG offers the additional advantage of the periodical variations, i.e. with the tangential position in the fluidization chamber, of the pressure and the gas-solid slip velocity. The periodical pressure and gas-solid slip velocity variations can be substantial and of very high frequency, depending on the type of particles and the particle bed rotational speed, and can be advantageous by enhancing interphase mass transfer, in particular for porous materials, and by interacting with cohesive inter-particle forces. The static geometry reduces, however, the freedom in design and operation of a RFB-SG, as, for a given fluidization chamber design and particle type, the gas flow rate and the particle bed rotational speed cannot be independently set.

Experimental Setup

The experimental setup at UCL-IMAP is shown in Figure 2 and consists of a compressor, a gas distribution device, a

Figure 2. Experimental setup.

(Vertical position shown.) Right, solids container and feeder; Center, from bottom to top: rotating fluidized bed apparatus, cyclone, bag filter; Back, gas distribution device; Left, solids recuperator. [Color figure can be viewed in the online issue, which is available at www.interscience.wiley.com.]

rotary valve, a solids container and feeder, the rotating fluidized bed apparatus, a cyclone, a filter, and a solids recuperator. The rotating fluidized bed apparatus, the cyclone, and the filter can be rotated around an axis, so that the fluidization chamber can be operated in the horizontal or the vertical (Figure 2) position. The rotating fluidized bed apparatus is constructed from three coaxial cylinders, which separate the medium fluidization chamber or reactor from the outer gas distribution chamber and from the inner chimney. As seen in Figure 3, the cylindrical design of the fluidization chamber is approximated by a polygonal design in the present investigation.

The compressor delivers a maximum air flow rate of 0.33 Nm^3/s and a maximum pressure of 182,340 Pa. Because of the pressure drop in the gas distribution section, the fluidization chamber, the cyclone, and the filter, the actual maximum gas flow rate through the experimental set-up is ± 0.2 m^3/s. The gas flow rate to the fluidization chamber can be controlled with a rotary valve. From the gas distribution device, the gas enters the 36 cm diameter, 13.5 cm long fluidization chamber via 12 tangential gas inlet slots in the cylindrical outer wall of the fluidization chamber. The width of the gas inlet slots is small (4 mm) to increase the tangential momentum injected for a given gas flow rate (Eq. 10), but sufficiently large to avoid an excessive pressure drop over the gas inlet slots. At the maximum gas flow rate of 0.2 m^3/s, the static pressure drop over the gas inlet slots is less than 4000 Pa. According to Eq. 7, the tangentially averaged radial gas velocity u_r in the fluidization chamber (which roughly corresponds to the radial gas-solid slip velocity) for a total gas flow rate of 0.2 m^3/s is $0.24/(r\ \varepsilon_g)$ m/s. Hence, assuming, for example, a solids volume fraction near the outer cylindrical wall of the fluidization chamber of 0.5, the tangentially averaged radial gas-solid slip velocity near the outer cylindrical wall of the fluidization chamber is about 2.8 m/s. Analogously, approaching the chimney where the solids volume fraction is very small, the tangentially averaged radial gas velocity is roughly 2 m/s. It should be remarked that the average residence time of the gas in the fluidization chamber is less than 6×10^{-2} s.

The solids flow rate is controlled by a volumetric screw feeder and a sealing rotary valve. The latter allows minimizing the risk of gas return from the fluidization chamber to the solids feeder and container. Downstream of the sealing rotary valve, the solids are pneumatically conveyed to the fluidization chamber. The solids enter the fluidization chamber via a solids inlet tube in one of the plexi-glass end plates of the fluidization chamber. Radially, the solids inlet tube is

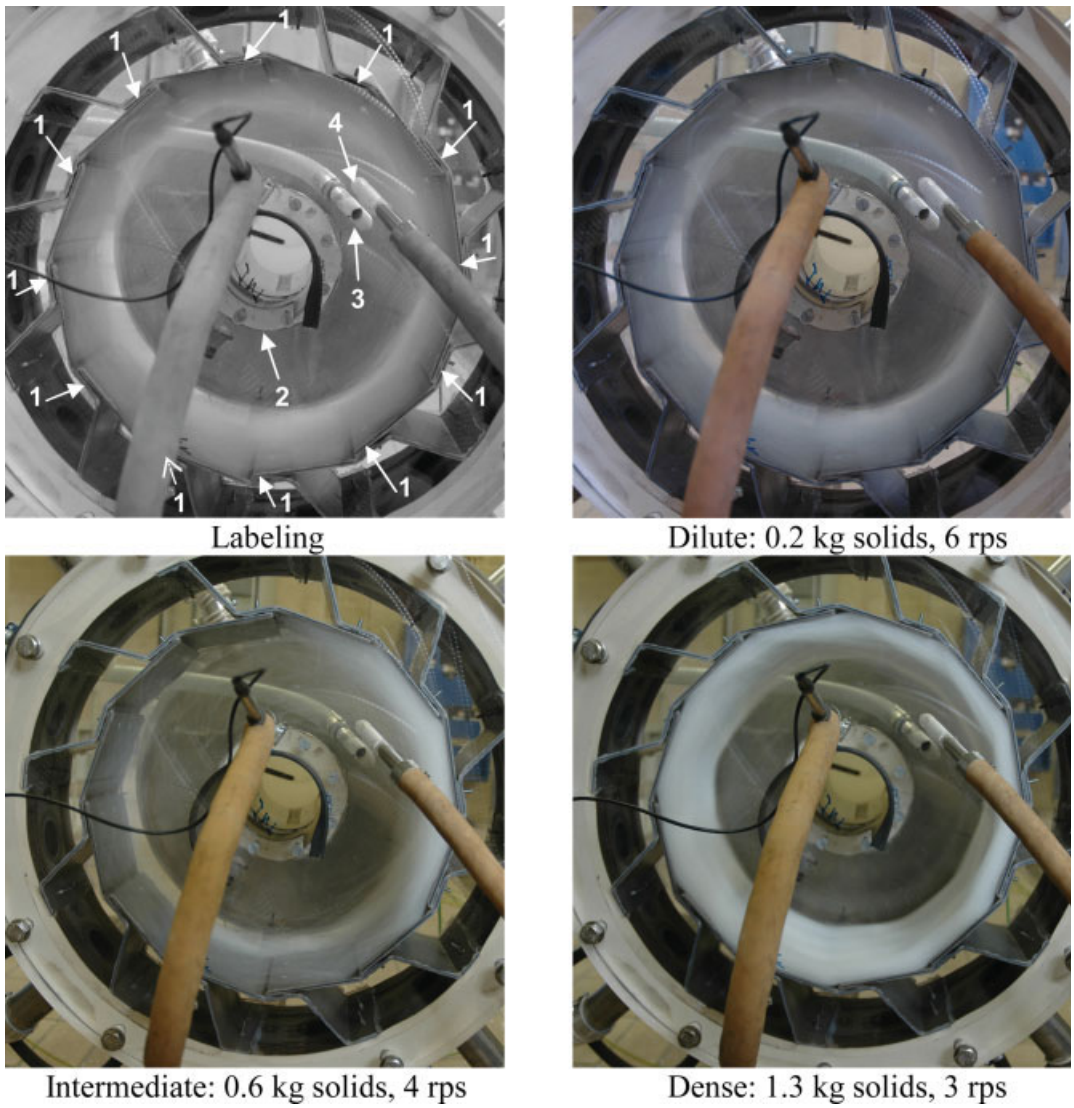

Figure 3. 1G-Geldart D particles: polymer, $\langle d_p \rangle$ = 2–5 mm (cylinders), ρ_p = 950 kg/m^3.

Horizontal operation. Total gas flow rate: 0.2 m^3/s. Conditions: see (a) in Table 1. Labeling: 1. gas inlet slot; 2. outlet to the chimney; 3. solids inlet; 4. solids outlet. [Color figure can be viewed in the online issue, which is available at www.interscience.wiley.com.]

positioned such that the solids enter in the dilute part of the fluidization chamber. To facilitate the tangential acceleration of the solids, the solids are fed in the tangential flow direction and the solids inlet tube makes a 30° angle with the plexi-glass end plate. The gas and eventually some solids (losses, fines) leave the fluidization chamber via an inner, quasi-centrally positioned, ±12 cm diameter chimney with, in the present case, a single, 9 cm width, outlet slot. Multiple outlet slots could be used as well. The single outlet slot design is, however, believed to offer some advantages, in particular with respect to the gas-solids separation in the fluidization chamber. This can be understood as follows. After the fluidization gas has moved radially inwards through the particle bed towards the chimney, it accumulates in a gas zone near the chimney, rotating towards the nearest chimney outlet slot (Figure 1b). Hence, in case there is only a single chimney outlet slot, the fluidization gas injected via the different tangential gas inlets gradually accumulates in the rotating gas zone near the chimney. As a result, maximum thickness of the gas zone and maximum tangential velocities are obtained immediately upstream the chimney outlet slot. Hence, in the rotating gas zone near the chimney, the centrifugal force is expected to be maximum immediately upstream the chimney outlet slot, improving the gas-solids separation and minimizing the solids losses via the chimney.

The gas that is removed from the fluidization chamber via the chimney is sent to a cyclone and a bag filter to remove eventual solids from the gas stream before sending it to the vent. The solids are removed from the fluidization chamber via a solids outlet tube in one of the plexi-glass end plates of the fluidization chamber. Radially, the solids outlet tube is positioned near the fluidized bed free-board. To facilitate the solids outflow, the solids outlet tube is oriented in the tangential flow direction, making a 30° angle with the plexi-

glass end plate. The solids are transported via a transfer leg to an expansion vessel where they are recuperated by gravity and from where they could be recycled to the solids feeder and the fluidization chamber. Neglecting solids losses via the chimney, the solids residence time in the fluidization chamber can be freely chosen and adjusted by controlling the solids inlet and outlet flow rate. The gas flow rate and the solids feeding/removal rate hardly influence the fluidized bed thickness or "height" (in the radial direction) that can be achieved, which is mainly determined by the solids outlet position.

The experimental setup, in particular the fluidization chamber design, is at this stage not optimal. The fluidization chamber dimensions (diameter, length, ...), the gas inlet slot geometry (slot width, inlet angle, ...), the gas inlet slot distribution, and the chimney and the chimney outlet(s) design, as well as the solids inlet and outlet, are to be optimized.[18] The optimal fluidization chamber design is expected to depend on the type of particles to be fluidized.

For the experimental proof of concept, one and the same nonoptimized fluidization chamber design is used to investigate the fluidization behavior with two different types of solids. The solid particle characteristics are summarized in Table 1. The 5 mm diameter, 2 mm long cylindrical polyethylene polymer particles with a particle density of 950 kg/m^3 behave like Geldart D-type particles in the earth gravitational field (1 G). It should be stressed that particles may behave like a different Geldart-type in a centrifugal field.[7] The size distribution of the polymer particles is quite narrow. The alumina particles have a mean particle size of 300 μm and a particle density of 2100 kg/m^3 and behave like Geldart B-type particles in the earth gravitational field (1 G). The particle size distribution of the alumina particles is determined by laser-diffractiometry and relatively broad. It should be noted that during continuous operation with the alumina particles, the mean particle size in the fluidization chamber is 400 μm rather than 300 μm, because of a preferential loss of fines via the chimney. The particle size distribution and the particle segregation in the fluidization chamber are discussed in more detail further in this study.

The fluidization behavior is studied visually and using normal and fast digital cameras. The fast digital camera and online PC allow taking, storing and analyzing pictures at up to 10,000 frames per second. Particular attention is paid to the behavior near the gas inlets (Figure 1b), where the important momentum and energy transfer between the gas and the solids takes place. The fast digital camera allows estimating the particle bed rotational speed. The solids feeding rate, the solids losses via the central chimney, and the amount of solids recuperated via the solids outlet are measured, allowing to determine the solids hold-up in the fluidization chamber. The total gas flow rate, the static pressure, and the temperature are measured immediately upstream of the gas distribution device. The static gas phase pressure drops over the gas inlet slots, the fluidization chamber, the chimney and cyclone, and the filter, can be measured using U-tube water manometers. At the maximum gas flow rate of 0.2 m^3/s, the static pressure drop over a gas inlet slot to the fluidization chamber is measured to be about 3700 Pa. At the same gas flow rate, the static pressure drop over a particle free fluidization chamber is about 6000 Pa, whereas the static pressure drop over the chimney and the cyclone is about 7600 Pa and the static pressure drop over a clean filter is about 4500 Pa.

Table 1. Experimental Conditions

	Unit	Value
Fluidization chamber diameter	[m]	36×10^{-2}
Fluidization chamber length	[m]	13.5×10^{-2}
Chimney diameter	[m]	$\pm 12 \times 10^{-2}$
Number of tangential gas inlet slots	[/]	12
Gas inlet slot width	[m]	4×10^{-3}
Total gas flow rate	[m^3/s]	0.2
Number of chimney outlet slots	[/]	1
Chimney outlet slot width	[m]	9×10^{-2}
Outlet pressure	[Pa]	101,300
Temperature	[K]	333
Number of solids inlets and outlets	[/]	1/1, via opposite end plates
Particle material	[/]	(a) polymer (b) alumina
Average particle size	[m]	(a) 2×10^{-3} (length), 5×10^{-3} (diameter) (cylinders) (b) 300×10^{-6} (original); 400×10^{-6} (fluidization chamber) (Figure 14)
Particle density	[kg/m^3]	(a) 950 (b) 2100
Solids loading	[kg]	(a) 0–2 (b) 0–1.5
Rotational speed (estimated)	[rps]	(a) 3–6 (b) 3–7

Experiments start with a particle free fluidization chamber. First, the gas flow rate to the fluidization chamber is set. Next, the particles are fed to the fluidization chamber (if wanted step wise) at a known flow rate. The fluidization chamber gradually fills with particles. If the solids outlet is open, particles start leaving the fluidization chamber via the solids outlet and a continuous, quasi-steady regime can be reached. If the solids outlet is closed, the fluidization chamber can be filled with particles up to the level where particles are lost via the central chimney outlet. Alternatively, with a closed solids outlet, the solids feeding can be stopped before losing particles via the chimney. Experiments can then be carried out with any chosen residence time of the particles in the fluidization chamber. This was done for preliminary attrition tests with the polymer particles.

Fluidization Behavior with Polymer Particles

Behavior at different solids loadings

Experiments are carried out with the solids outlet closed. The fluidization chamber is gradually filled with polymer particles (a) in Table 1 at an almost constant total gas flow rate, which approaches the maximum possible total gas flow rate of about 0.2 m^3/s. From a fast camera picture analysis, the rotational speed of the fluidized bed is estimated between 3 and 6 rps, respectively for the highest and the

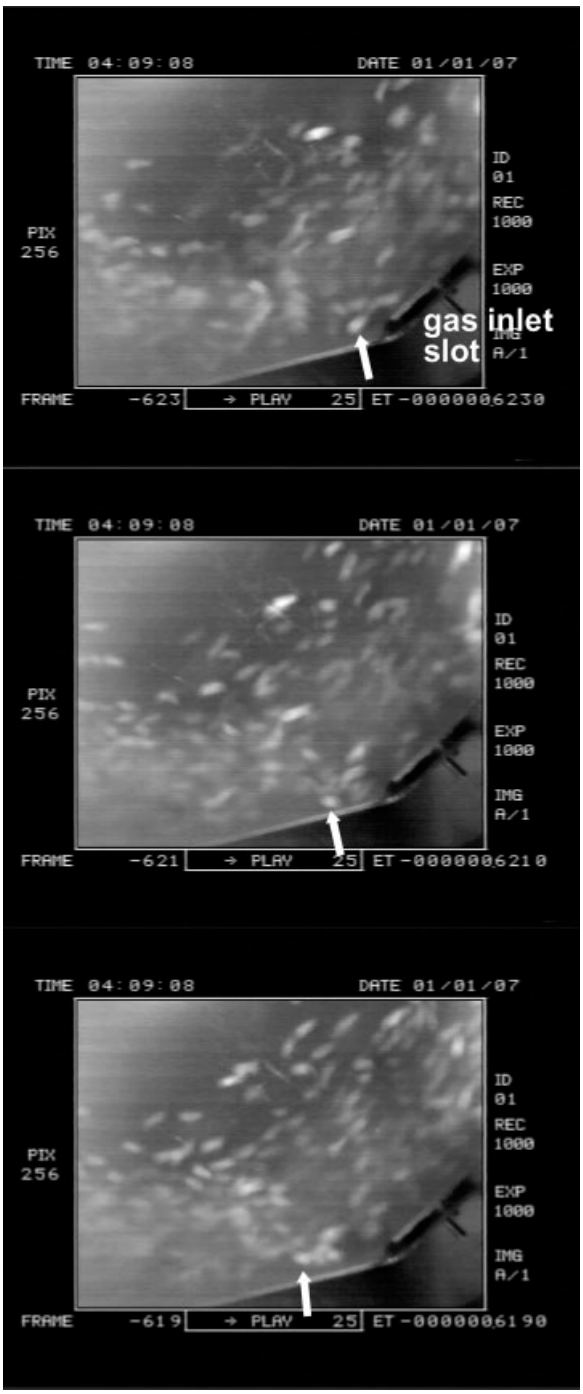

Figure 4. Fast digital camera analysis of the motion of 1G-Geldart D particles near a tangential gas inlet slot of the fluidization chamber.

Illustration of particle tracking and particle-wall collisions (see arrow). Particles: polymer, $\langle d_p \rangle$ = 2–5 mm (cylinders), ρ_p = 950 kg/m^3. Horizontal operation. Total gas flow rate: 0.2 m^3/s. Solids loading: 0.2 kg. Rotational speed: 6 rps. Conditions: see (a) in Table 1. Time interval Δt between frames shown: 2×10^{-3} s.

lowest solids loading. At the outer cylindrical wall of the fluidization chamber, the corresponding centrifugal acceleration is roughly between 7 and 26 G. This is low compared to the rotational speeds at which conventional RFB usually operate (10–300 G).[1–15] Straightforward strategies to obtain higher rotational speeds are either increasing the total gas flow rate or reducing the fluidization chamber volume.

The behavior of the RFB-SG observed at different solids loadings is shown in Figure 3. At low solids loadings (0.2 kg in Figure 3), a quite uniform dilute rotating fluidized bed is observed. The particle motion is complex and collisions between the particles and the solid walls, mainly the outer cylindrical side wall, of the fluidization chamber are important. Because of the centrifugal force, the gas-solids separation is, however, excellent with no particle losses via the chimney outlet. As the solids loading increases (0.3–0.5 kg, not shown in Figure 3), particle-particle collisions become more important and, as a result of the centrifugal force, a densification, i.e. an accumulation of particles, near the cylindrical side wall of the fluidization chamber is observed. A dense particle bed forms near the outer cylindrical wall of the fluidization chamber. More inwards, the particle bed gradually becomes less dense and the gas-solids separation remains excellent with no particle losses via the chimney. Figures 4 and 5 show details of the rotating fluidized bed behavior in the vicinity of a tangential gas inlet slot at respectively solids loadings of 0.2 and 0.5 kg. The pictures are taken with a fast digital camera at 1000 frames per second. The particle motion in the rotating fluidized bed is seen to be very vigorous and complex and the particles are well-mixed. The fast digital camera technique allows to track particles and to estimate the bed rotational speed. Figure 4 (arrows), for example, illustrates a particle-wall collision. All fast digital camera measurements are taken perpendicularly through the plexi-glass end plates. Visual and normal camera observations (Figures 3 and 7) show, however, that the inner surface of the rotating fluidized bed exhibits the same behavior observed with the fast digital camera. No accumulation

Figure 5. Fast digital camera analysis of the motion of 1G-Geldart D particles near a tangential gas inlet slot of the fluidization chamber.

Illustration of the vigorous motion in the rotating fluidized bed. Particles: polymer, $\langle d_p \rangle$ = 2–5 mm (cylinders), ρ_p = 950 kg/m^3. Horizontal operation. Total gas flow rate: 0.2 m^3/s. Solids loading: 0.5 kg. Rotational speed: 5 rps. Conditions: see (a) in Table 1.

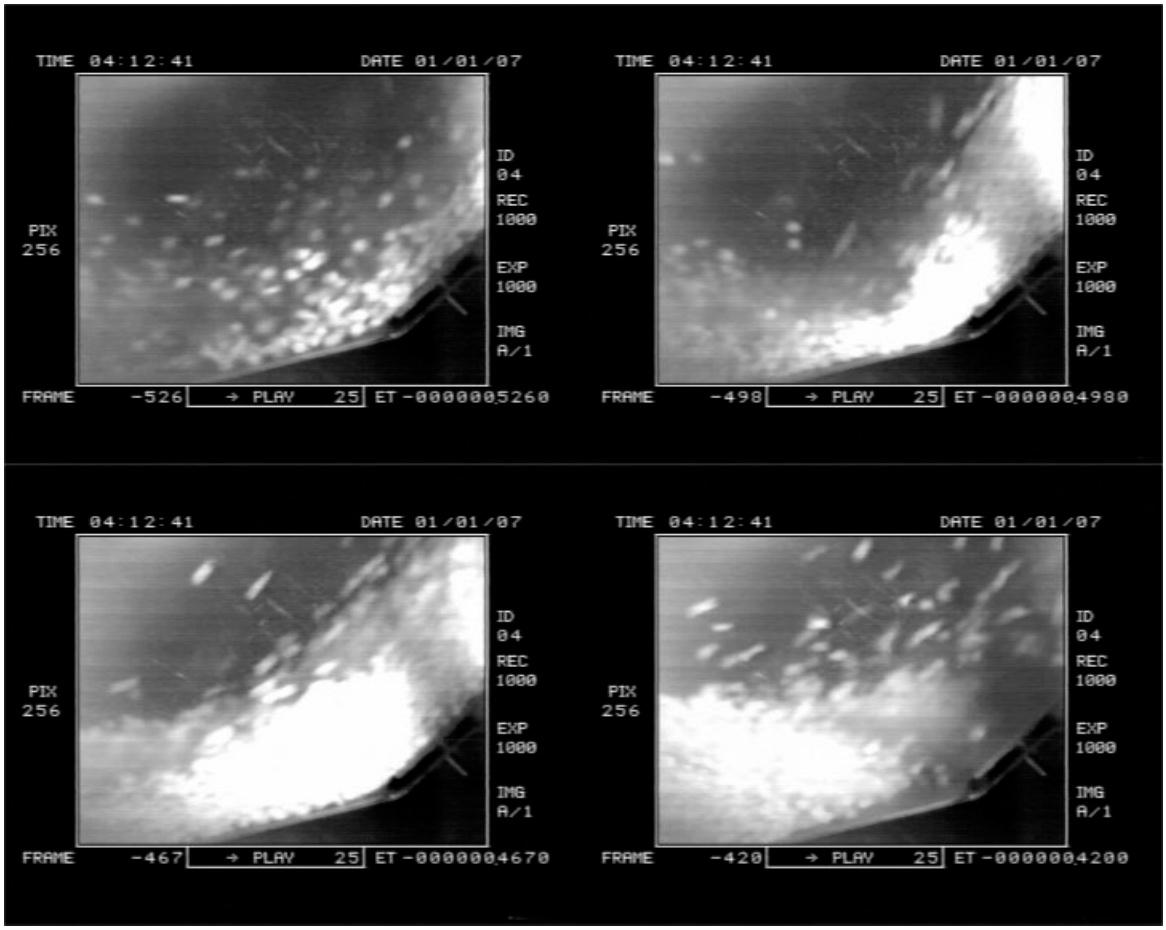

Figure 6. Fast digital camera analysis of the motion of 1G-Geldart D particles near a tangential gas inlet slot of the fluidization chamber.

Illustration of slugging. Particles: polymer, $\langle d_p \rangle$ = 2–5 mm (cylinders), ρ_p = 950 kg/m^3. Horizontal operation. Total gas flow rate: 0.2 m^3/s. Solids loading: 0.6 kg. Rotational speed: 4 rps. Conditions: see (a) in Table 1. Time interval Δt between frames shown: $\pm 30 \times 10^{-3}$ s.

of polymer particles sticking to the plexi-glass end plates is seen in any of the experiments, indicating that electrostatic forces for the large polymer particles are negligible.

At solids loadings of 0.3–0.5 kg, channeling may occur (not shown; shown for the alumina particles further in this study). In such case, the particles rotate preferentially at one side, that is, near one of the end plates, of the fluidization chamber and the gas bypasses via the other side, that is, near the other end plate, of the fluidization chamber. Hence, the particle distribution is strongly nonuniform in the longitudinal direction of the fluidization chamber. In case channeling occurs, the particle bed height increases locally and, as a result, close to the end plate, where the increase of the bed height is the most pronounced, particle losses via the chimney outlet may occur. This may disturb further filling of the fluidization chamber with particles and limit as such the solids hold-up in the fluidization chamber. Channeling is enhanced as there is no controlled uniform distribution of the gas flow rate over a gas inlet slot. Only the total gas flow rate is controlled in the experiment.

As the solids loading increases further (0.6 kg in Figure 3), slugging is observed (probably corresponding to an eigenmode of the system). The solids are distributed evenly in the longitudinal direction of the fluidization chamber, but a strongly nonuniform tangential distribution of the solids in the fluidization chamber occurs, that is, a solids slug rotates in the fluidization chamber. As with channeling, gas bypassing dense particle zones enhances slugging. In the experiment, only the total gas flow rate is controlled and not the distribution of the gas flow rate over the different gas inlet slots. As a result, in the slugging regime, the gas flow rate through a gas inlet slot drops sharply when the solids slug passes by, the gas entering the fluidization chamber preferentially via the other gas inlet slots that do not face the resistance of a solids bed. Slugging is most probably related to a poor radial fluidization of the particle bed. Figure 6 shows a fast digital camera record of slugging. As seen from the last frame in Figure 6, the gas flow rate through the gas inlet slot returns after the slug has passed by, lifting the end of the slug. Because of the relatively high frequency of the slugging phenomenon ($\pm$4 Hz), controlling the gas flow rates to the different gas inlet slots with standard flow rate controllers may be difficult. An experiment in which the gas is distributed via the bottom and upward pointing gas inlet slots only, the other gas inlets being closed with valves, shows that a smart distribution of the gas allows removing slugging, but

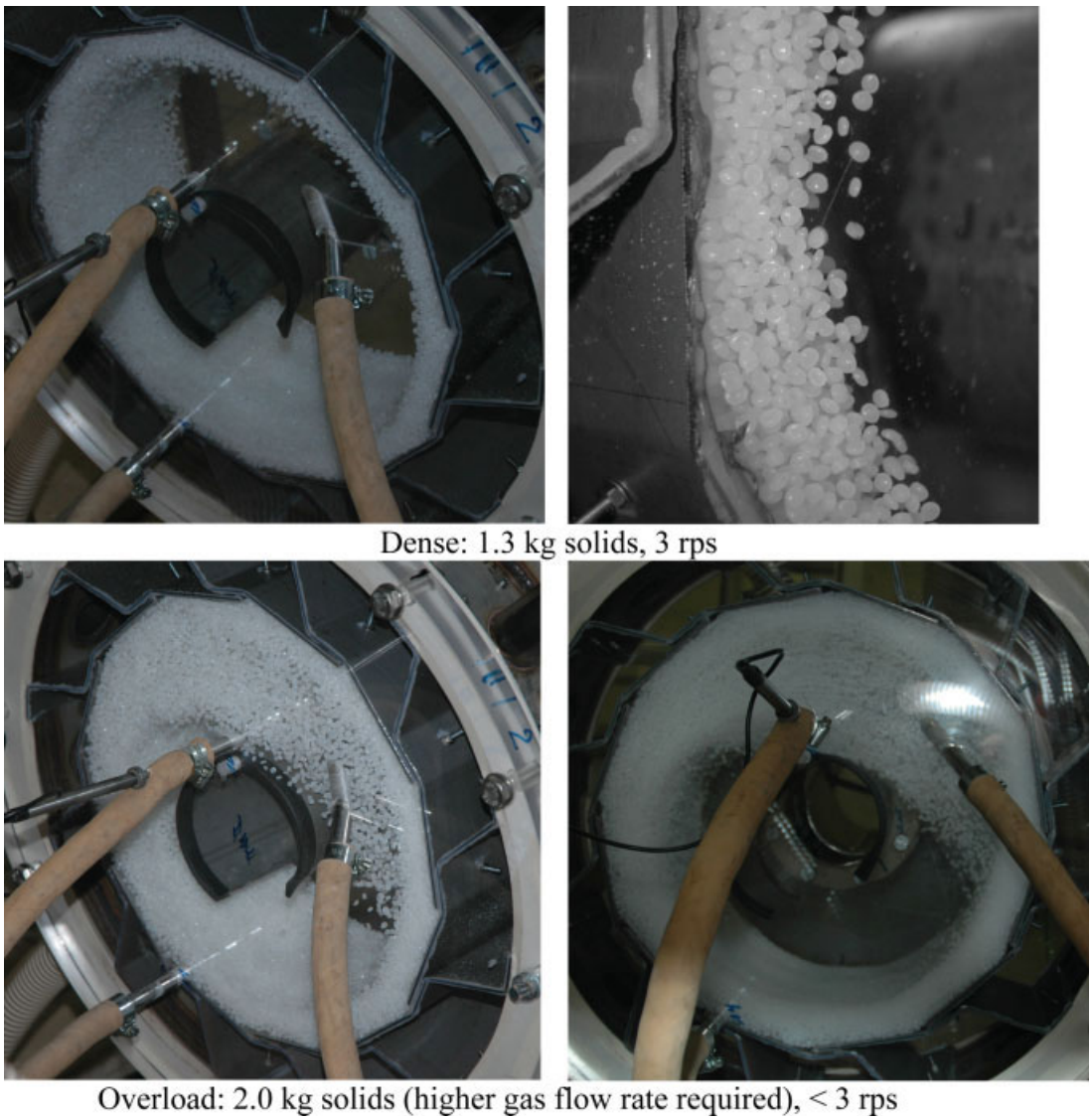

Figure 7. 1G-Geldart D particles: polymer, $\langle d_p \rangle$ = 2–5 mm (cylinders), ρ_p = 950 kg/m^3.

Horizontal operation. Total gas flow rate: 0.2 m^3/s. Conditions: see (a) in Table 1. [Color figure can be viewed in the online issue, which is available at www.interscience.wiley.com.]

doing so some channeling occurs. Furthermore, a redistribution of the (fluidization) gas over the different gas inlet slots has its limitations, such a redistribution not only affecting the rotational and longitudinal motion of the particles, but also their radial motion, i.e. the radial fluidization. Alternative ways of controlling channeling and slugging are investigated. It should be remarked that slugging may also occur at lower solids loadings if the total gas flow rate, and as a result the rotational speed, is reduced.

At higher solids loadings and provided that the bed rotational speed is sufficiently high (1.3 kg in Figures 3 and 7), slugging disappears and the polymer particles form a stable, dense, uniform rotating fluidized bed. This transition is quite abrupt. The snap-shot in Figure 7 may give the impression of a (rotating) fixed bed, as obtained in conventional RFB below the minimum fluidization gas flow rate, but the particle bed is (mainly tangentially) fluidized and, as seen from Figure 3 with a larger exposure time, the particle motion is complex and vigorous. As a result of the combination of the tangential and some radial motion, the particles are well-mixed. The assumption of a solid body rotation of the particle bed seems on average, however, justified.

With the current fluidization chamber design, at high solids loadings, the radial fluidization or bed expansion with the polymer particles is rather limited, despite the high radial fluidization gas velocities (radial gas-solid slip velocities of at least 2 m/s). In fact, the detail snap-shot in Figure 7 shows that the freeboard of the rotating fluidized bed only is truly radially fluidized, in agreement with the layered fluidization observed in conventional RFB.[8] Hence, for the polymer particles ((a) in Table 1), with the current fluidization chamber design, the ratio of the tangential, and the radial velocities, so i.e. the ratio of the centrifugal force and the radial drag force, is too high and the radial gas velocity is close to the surface minimum fluidization velocity. As a result, the gas-

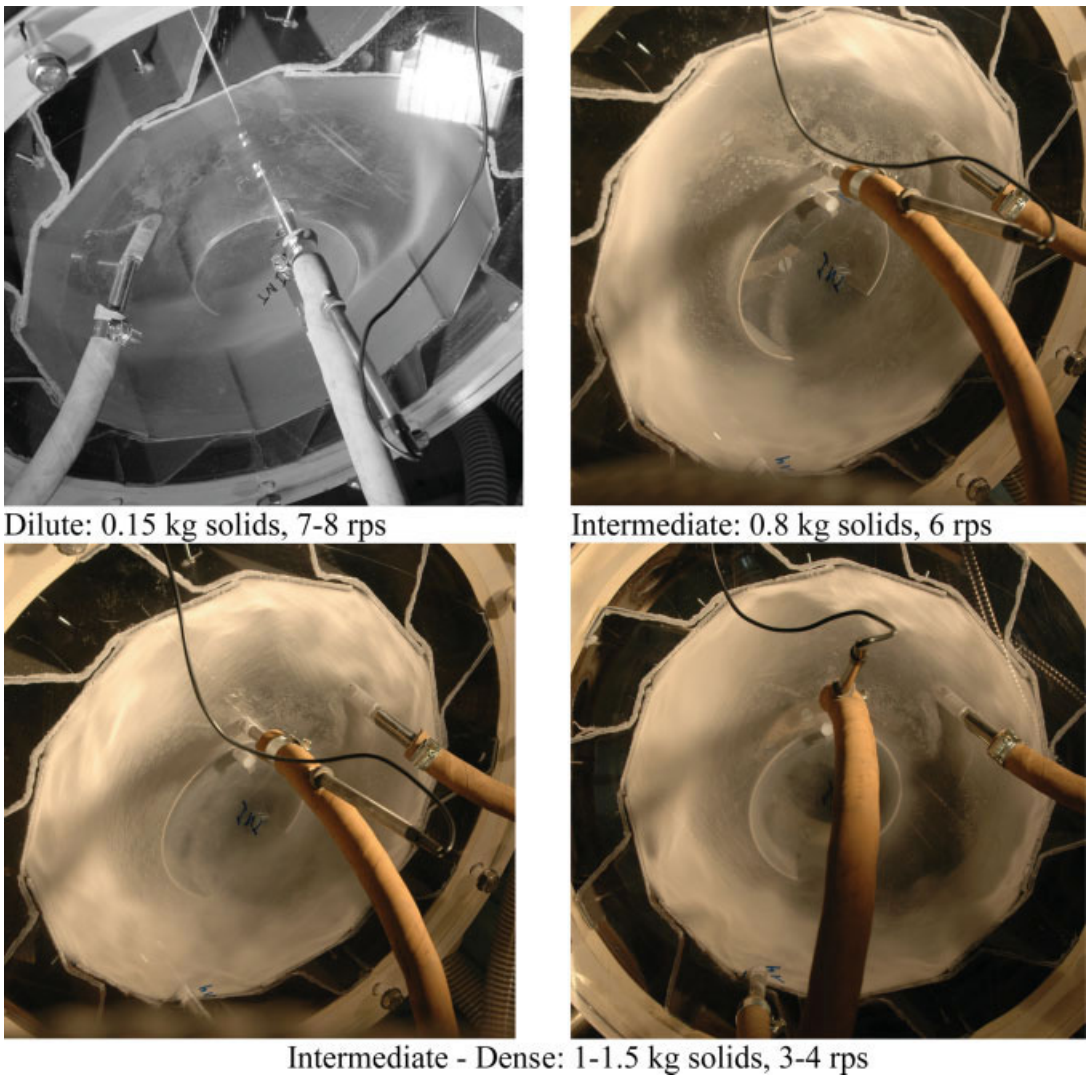

Figure 8. 1G-Geldart B particles: Alumina, $\langle d_p \rangle$ = 400 μm (*), ρ_p = 2100 kg/m^3.

Horizontal operation. Total gas flow rate: 0.2 m^3/s. Conditions: see (b) in Table 1. (*) In the fluidization chamber; 300 μm for the original Alumina particles fed (see Figure 14). [Color figure can be viewed in the online issue, which is available at www.interscience.wiley.com.]

solid separation is very good with no particle losses via the chimney. The solids outlet being closed in the experiment, the solids feeding can be stopped to obtain a hydrodynamically steady-state operation. To increase the radial fluidization with the polymer particles, the fluidization chamber design can be adapted, in particular its dimensions, the gas inlet slot geometry, the number of gas inlet slots and their distribution, and/or the gas inlet angle. For example, as explained earlier, keeping the fluidization chamber volume and length fixed, the outer (R) and inner (chimney) radius of the fluidization chamber can be reduced.

Figure 7 shows the rotating fluidized bed behavior at a solids loading of 2.0 kg. At this solids loading, the maximum deliverable gas flow rate and tangential momentum injected are insufficient, that is, the bed rotational speed and, hence, the centrifugal force, become too low to dominate gravity. As a result, in the horizontal operation, the particles are seen to fall down in the top of the fluidization chamber (Figure 7). It should be noticed that even at this point, the particle losses via the chimney are minimal, the chimney outlet slot being positioned at the bottom of the fluidization chamber (Figure 7). In the vertical operation (not shown), however, the particle bed is observed to form an angle with the vertical axis at too high solids loadings and too low rotational speeds and, at this point, particle losses via the chimney may occur at the bottom of the fluidization chamber. Higher gas flow rates reduce the effects of gravity.

Qualitative experimental observations at different gas flow rates between 0.1 and 0.2 m^3/s (not shown) give a first confirmation of a fluidization behavior relatively independent of the gas flow rate and, hence, the possibility of a relatively broad operation range, except when gravity effects become important.

At the experimental conditions of Table 1, the static pressure drop over a particle free fluidization chamber is about 6000 Pa. With a rotating fluidized bed of the polymer particles, the static pressure drop over the fluidization chamber is less than 8000 Pa at low solids loading (Figure 3, 0.2 kg

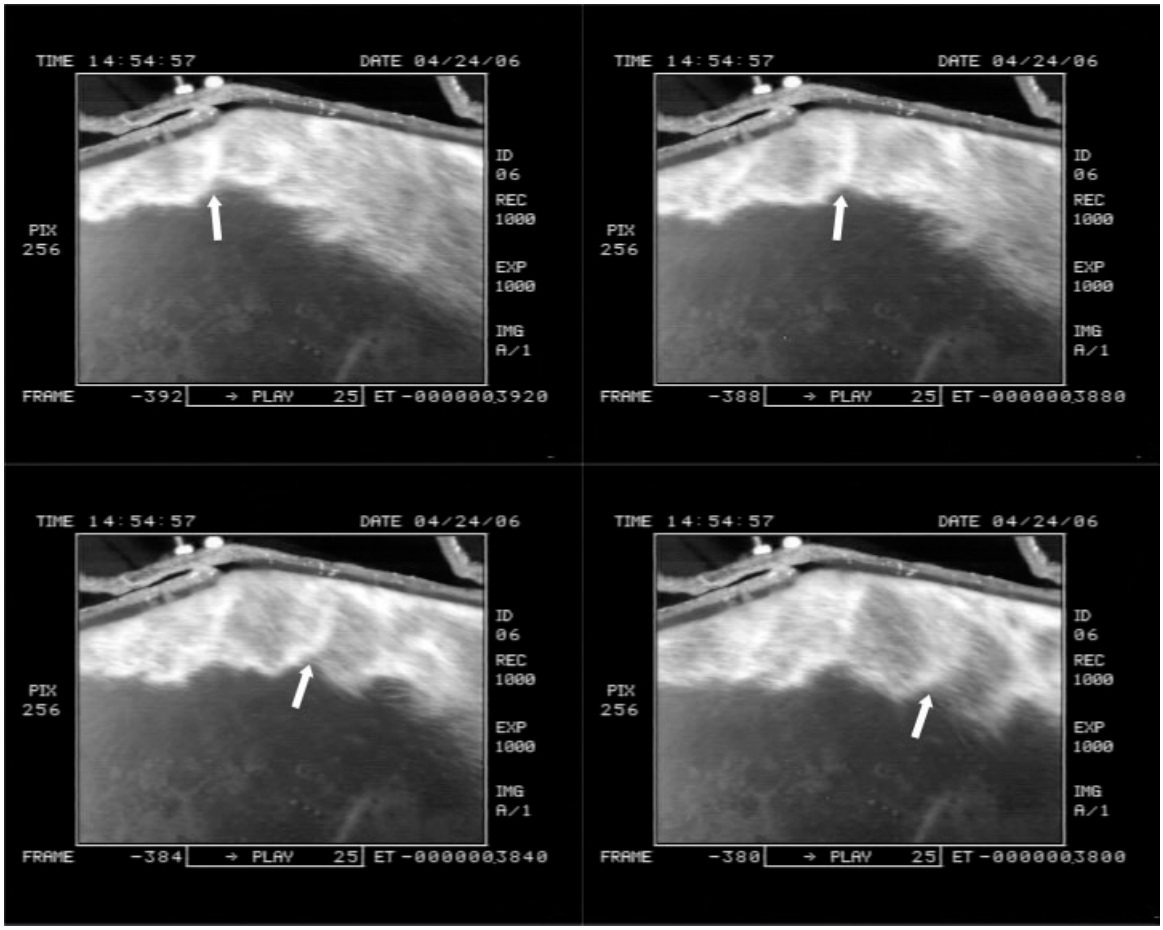

Figure 9. Fast digital camera analysis of the motion of 1G-Geldart B particles near a tangential gas inlet slot of the fluidization chamber.

Illustration of particle wave formation and propagation (see arrow). Particles: Alumina, $\langle d_p \rangle$ = 400 μm (*), ρ_p = 2100 kg/m^3. Horizontal operation. Total gas flow rate: 0.2 m^3/s. Solids loading: 0.6 kg. Rotational speed: 6 rps. Conditions: see (b) in Table 1. Time interval Δt between frames shown: 4×10^{-3} s. (*) In the fluidization chamber; 300 μm for the original Alumina particles fed (see Figure 14).

solids) and less than 20,000 Pa at the highest solids loading (Figure 3, 1.3 kg).

Continuous operation

An experiment is carried out (not shown) to verify the possibility of a continuous operation with the solids outlet opened. The solids are easily removed from the fluidization chamber via the solids outlet and recuperated in the expansion vessel. This allows a continuous recycle or regeneration of the solids. While continuously feeding and removing particles, a hydrodynamically steady-state is automatically established when the rotating fluidized bed freeboard reaches the position of the solids outlet (at about 1.8 kg solids loading). The conceptually straightforward and practical particle feeding and removal to and from the fluidization chamber is an important advantage of the RFB-SG.

Attrition

Attrition by shear as a result of particle-particle and particle-wall collisions may be a concern when using the RFB-SG in practice. Therefore, a preliminary attrition test with the polymer particles is carried out. The solids outlet is closed and 1.8 kg of particles is fed to the fluidization chamber operating at the maximum gas flow rate of 0.2 m^3/s. With zero particle losses via the chimney, the particles are kept in the rotating fluidized bed for 3 h, that is, the particle residence time is 3 h. The losses of fines in the cyclone and the filter after the 3-h operation period are measured to be about 0.4 g. Hence, from this preliminary test, for the polymer particles, the losses of fines due to attrition are found to be very limited.

Fluidization Behavior with Alumina Particles

Behavior at different solids loadings

Figure 8 shows the rotating fluidized bed behavior obtained with the Alumina 1G-Geldart B-type particles at different solids loadings. The operating conditions and particle properties are summarized as (b) in Table 1. During the experiment, the solids outlet is closed, allowing to set the solids loading in the fluidization chamber more easily. From

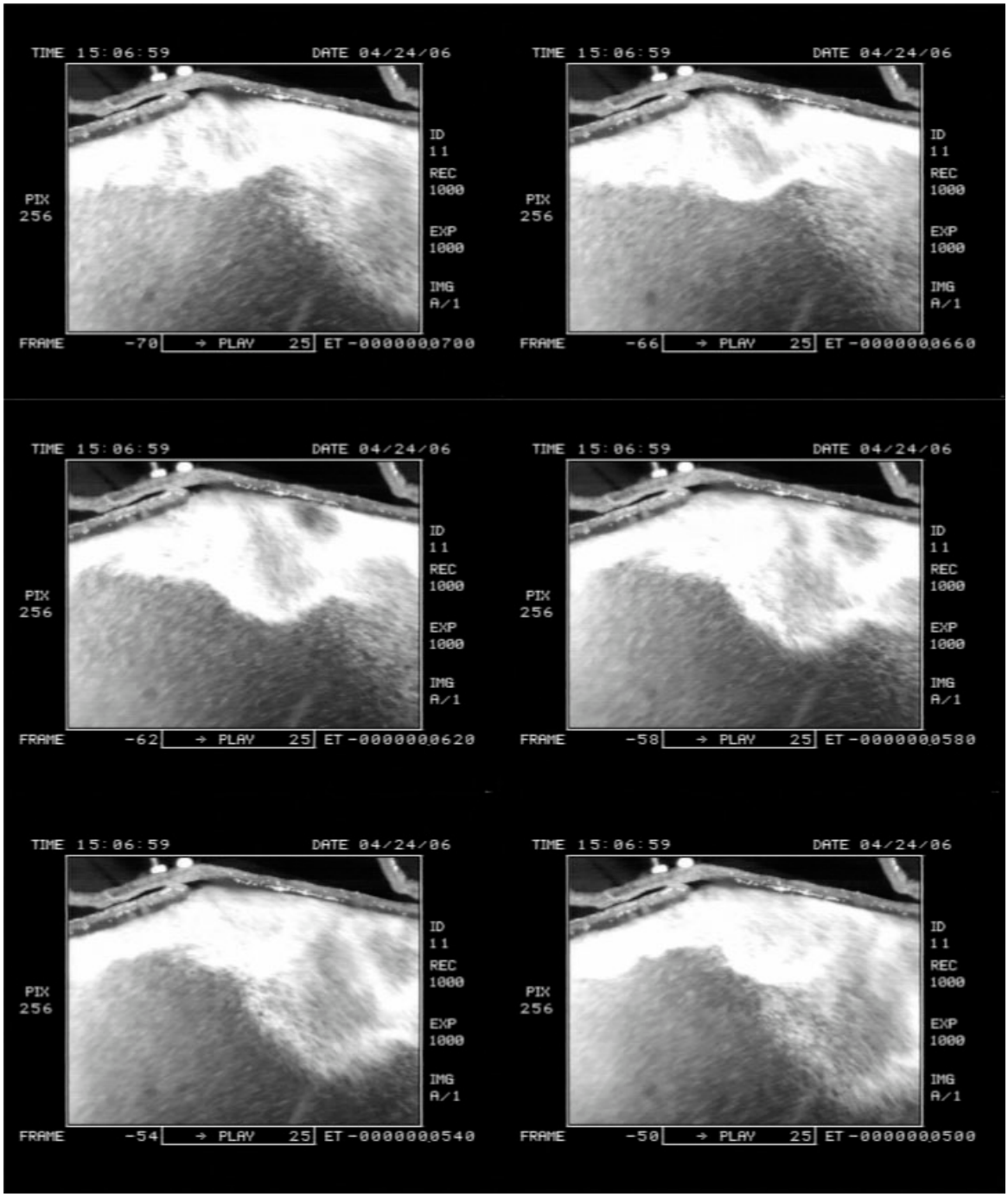

Figure 10. Fast digital camera analysis of the motion of 1G-Geldart B particles near a tangential gas inlet slot of the fluidization chamber.

Illustration of bubble formation, propagation, and growth. Particles: Alumina, $\langle d_p \rangle$ = 400 μm (*), ρ_p = 2100 kg/m^3. Horizontal operation. Total gas flow rate: 0.2 m^3/s. Solids loading: 0.8 kg. Rotational speed: 4.5 rps. Conditions: see (b) in Table 1. Time interval Δt between frames shown: 4×10^{-3} s. (*) In the fluidization chamber; 300 μm for the original alumina particles fed (see Figure 14).

a fast camera picture analysis, the particle bed rotational speed under the operating conditions of (b) in Table 1 was estimated to be between 3 and 8 rps, respectively for the highest and the lowest solids loading.

At low solids loadings (0.15 kg in Figure 8), channeling, i.e. gas bypassing zones of higher solids density, occurs, resulting in a longitudinally strongly nonuniform rotating fluidized bed. The solids are seen to rotate at one side of the fluidization chamber, close to the end plate in the back in Figure 8, whereas the gas is bypassing via the other side of the fluidization chamber. The role of the solids feeder design in the occurrence of channeling is to be further investigated,

but most probably channeling in a certain low solids loading range is intrinsic to the RFB-SG.

At higher solids loadings (0.8 kg and 1.0–1.5 kg in Figure 8), the solids are longitudinally more evenly distributed. The rotating fluidized bed behavior at higher solids loadings is very different with the alumina particles (Figure 8) than with the polymer particles (Figures 3 and 7). With the alumina particles, the rotating fluidized bed is less dense and less uniform than with the polymer particles. Furthermore, the rotating fluidized bed is much more agitated and the radial fluidization is much more pronounced. As a result of the radial bed expansion, the freeboard of the rotating fluidized bed is positioned rather close to the chimney and particle losses via the chimney outlet are quite pronounced with the Alumina particles, whereas absent with the polymer particles. Hence, although the solids outlet is closed in the experiment, continuous solids feeding is necessary to operate the fluidization chamber at a constant solids loading. After keeping the solids loading in the fluidization chamber constant at about 1.5 kg over a 10 min period, roughly 2.5 kg solids are recuperated via the cyclone and the filter. The particle residence time is, however, difficult to determine. On the basis of the visual observations, the particle residence time distribution is believed to be broad and complex. Accurate particle residence time measurements are to be carried out.

An optimization of the fluidization chamber design can reduce the particle losses via the chimney. For example, as explained earlier, keeping the fluidization chamber volume and length fixed the ratio of the centrifugal force and the gas-solid drag force can be increased by increasing the outer (R) and inner (chimney) radius of the fluidization chamber.

Fast digital camera pictures taken at 1000 frames per second allow getting an improved insight in the complex behavior of the rotating fluidized bed and the nonuniformities that occur, in particular in the vicinity of the gas inlet slots. All fast digital camera measurements are taken perpendicularly through the plexi-glass end plates. Visual and normal camera observations (Figure 8) show, however, that the inner surface of the rotating fluidized bed exhibits the same behavior observed with the fast digital camera. Little accumulation of alumina particles sticking to the plexi-glass end plates is seen in any of the experiments, indicating that electrostatic forces for the relatively large alumina particles are of limited importance. At a low solids loading (0.6 kg) (Figure 9), a wavy solids pattern is observed. The waves are mainly tangentially propagated (see arrows in Figure 9). Also, the assumption of a solid body rotation of the particle bed seems on average justified. At somewhat higher solids loadings (0.8 kg) (Figure 10), bubble formation is seen to occur. Gas bubbles originate near the gas inlet slots at the outer cylindrical wall of the fluidization chamber and propagate both tangentially and radially in the rotating fluidized bed. The bubble size is seen to increase considerably as the bubbles propagate towards the freeboard surface of the rotating fluidized bed. Bubbling was also observed in conventional RFB,[3] in which at low rotational speeds the fluidization efficiency was seen to decrease with increasing gas velocity due to bubble bypassing. Bubbles were, however, shown to play an important role in radial mixing in conventional RFB.[11] Furthermore, the bubble path was shown to deflect from a purely radial path by the Coriolis force.[15] The dynamics of isolated bubbles and bubble swarms in conventional RFB was theoretically investigated by Chevray et al.,[15] showing that the fraction of gas captured in bubbles increases considerably

Figure 11. Fast digital camera analysis of the motion of 1G-Geldart B particles near a tangential gas inlet slot of the fluidization chamber.

Illustration of bubble formation and growth, stretching, and propagation (encircled). Particles: Alumina, $\langle d_p \rangle$ = 400 μm (*), ρ_p = 2100 kg/m^3. Horizontal operation. Total gas flow rate: 0.2 m^3/s. Solids loading: 1.1 kg. Rotational speed: 3.5 rps. Conditions: see (b) in Table 1. Time interval Δt between frames shown: 8×10^{-3} s. (*) In the fluidization chamber; 300 μm for the original Alumina particles fed (see Figure 14).

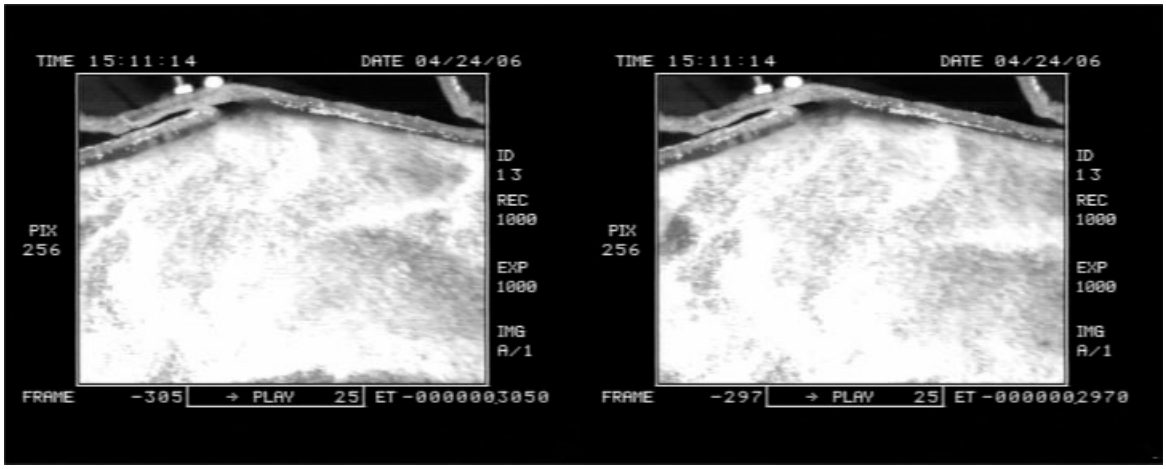

Figure 12. Fast digital camera analysis of the motion of 1G-Geldart B particles near a tangential gas inlet slot of the fluidization chamber.

Illustration of rotating fluidized bed at high solids loading. Particles: Alumina, $\langle d_p \rangle$ = 400 μm (*), ρ_p = 2100 kg/m^3. Horizontal operation. Total gas flow rate: 0.2 m^3/s. Solids loading: 1.5 kg. Rotational speed: 3.5 rps. Conditions: see (b) in Table 1. Time interval Δt between frames shown: 8×10^{-3} s. (*) In the fluidization chamber; 300 μm for the original Alumina particles fed (see Figure 14).

with decreasing radius, that is as the bubbles approach the fluidized bed freeboard surface. The present observations show that the same holds for bubbles in RFB-SG.

It should be remarked that the density of the rotating fluidized bed decreases when going radially inwards in the fluidization chamber. Figure 10 shows two distinct zones in the rotating fluidized bed. Near the outer cylindrical wall of the fluidization chamber, a dense rotating fluidized bed is observed, whereas a quite dilute rotating fluidized bed is observed more radially inwards. The transition between the two zones is quite abrupt. As the solids loading increases further (1.1 kg) (Figure 11), bubble formation still occurs, but the bubble growth is less pronounced and the bubbles propagate somewhat more tangentially than radially. This could be due to the growing "weight" of the particle bed in the centrifugal field. The latter is confirmed at higher solids loadings (1.5 kg) (Figure 12). At such high solids loadings, nonuniformities in the rotating fluidized bed are propagated mainly tangentially and, as a result, their residence time in the rotating fluidized bed is prolonged. Figure 11 also demonstrates bubble stretching. The latter could indicate a non-solid body type of rotation of the fluidized bed as its freeboard surface is approached. Investigating conventional RFB, Chevray et al.[15] showed that at high gas velocities, in the inner part of the fluidized bed, the motions of large bubbles could possibly induce nonsolid body types of rotation.

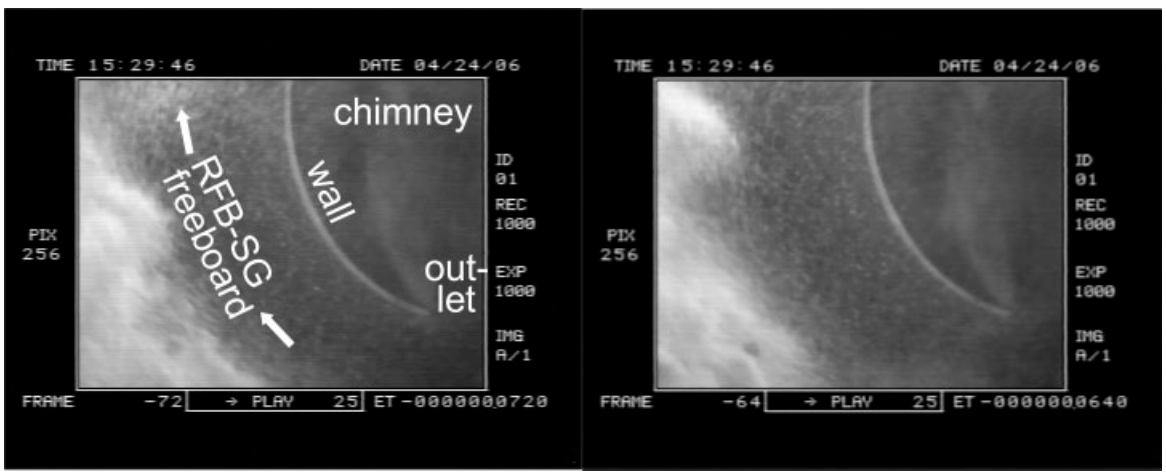

Figure 13. Fast digital camera analysis of the motion of 1G-Geldart B particles in the freeboard region of the rotating fluidized bed near the chimney, right downstream of the chimney outlet slot.

Particles: Alumina, $\langle d_p \rangle$ = 400 μm (*), ρ_p = 2100 kg/m^3. Horizontal operation. Total gas flow rate: 0.2 m^3/s. Solids loading: 1.5 kg. Rotational speed: 3.5 rps. Conditions: see (b) in Table 1. Time interval Δt between frames shown: 8×10^{-3} s. (*) In the fluidization chamber; 300 μm for the original Alumina particles fed (see Figure 14).

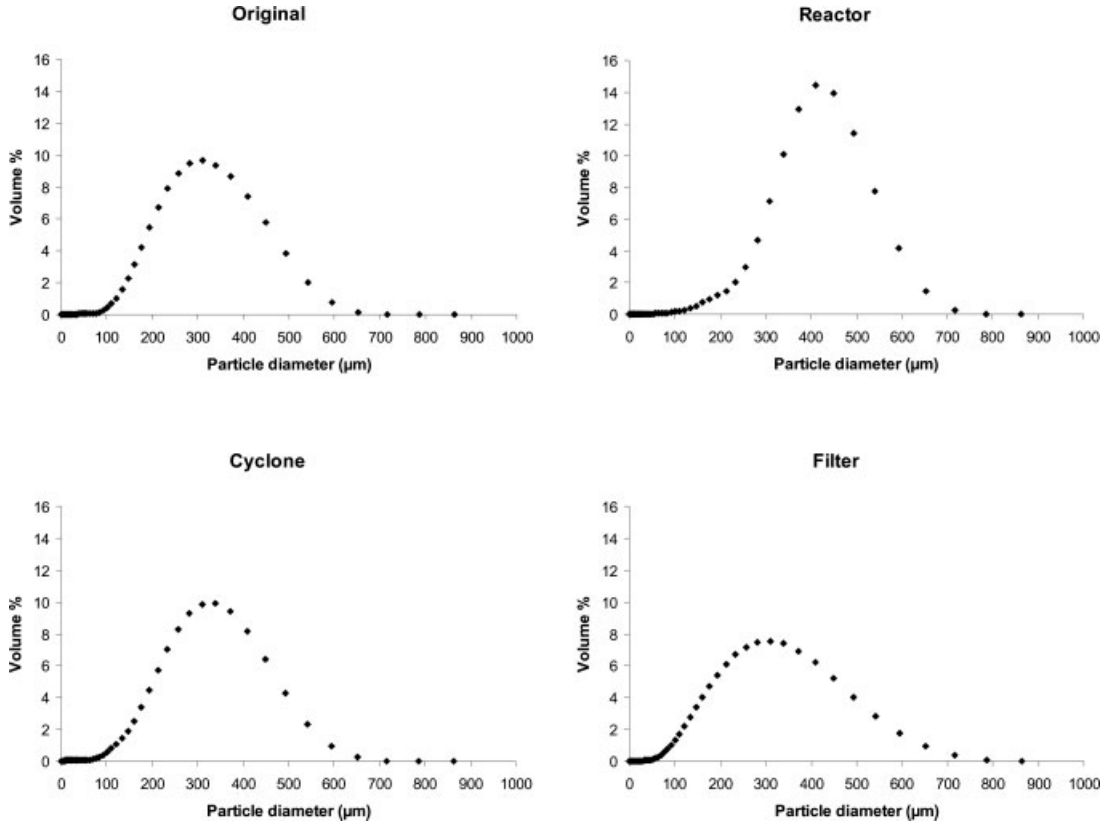

Figure 14. Normalized particle size distributions during continuous operation.

Qualitative (v) picture of particle segregation/classification in the fluidization chamber and cyclone. 1G-Geldart B particles: Alumina, $\langle d_p \rangle$ = 400 μm (*), ρ_p = 2100 kg m^{-3}. Horizontal operation. Solids loading: 1–1.5 kg. Total gas flow rate: 0.2 m^3/s. Rotational speed: 3–4 rps. Conditions: see (b) in Table 1. (v) Particle residence time in the fluidization chamber not quantified. (*) In the fluidization chamber; 300 μm for the original Alumina particles fed.

Figure 13 shows fast digital camera pictures of the freeboard surface of the rotating fluidized bed near the chimney outlet. Despite the vigorous motion of the rotating fluidized bed, the gas-solid separation near the chimney is quite good. Still, particle losses via the chimney are considerable in this case. This is also due to local vortex formation immediately downstream of the chimney outlet in the gas zone near the chimney. The small vortex observed creates recirculation, i.e. counter-flow along the chimney, entraining solids from the fluidized bed freeboard surface to the chimney outlet. The visual and fast digital camera observations near the chimney confirm that the assumption of a solid body rotation does not hold for the entire fluidization chamber. Whereas in the dense particle bed region near the outer cylindrical wall of the fluidization chamber the solid body rotation assumption for the particle bed seems on average justified (e.g. Figures 9 and 12), more towards the fluidized bed freeboard surface and further inwards in the gas zone near the chimney, zones of irrotational motion (free vortex), and dissipative rotational motion (forced vortex) seem to exist. This behavior is similar to the behavior in conventional RFB.[15]

Whereas, at the experimental conditions of Table 1, the static pressure drop over a particle free fluidization chamber is about 6000 Pa, with a rotating fluidized bed of the alumina particles, the static pressure drop over the fluidization chamber is less than 7000 Pa at low solids loading (Figure 8, 0.15 kg solids) and less than 20,000 Pa at the highest solids loading (Figure 8, 1–1.5 kg).

Particle segregation

Figure 14 qualitatively illustrates particle segregation or classification, that is, the separation of particles of different size, in the fluidization chamber and in the cyclone. Particle size distributions are measured of samples taken from the solids feeding container ("original" in Figure 14), the fluidization chamber, the cyclone, and the filter during continuous operation of the rotating fluidized bed. Because of the considerable particle losses via the chimney and due to the lack of information on the particle residence time and its distribution, a quantification of the particle segregation in the fluidization chamber, e.g. a relation with the particle residence time, could not be made so far. The qualitative picture is, however, clear: small particles are more easily entrained via the chimney outlet of the fluidization chamber than large particles. Compared to the original particle size distribution, the particle size distribution in the fluidization chamber shows a larger mean particle size. Furthermore, the particle size distribution curve has narrowed. The observed particle segregation in the fluidization chamber is, however, not very pronounced or sharp. The behavior

observed is in agreement with theoretical predictions of the elutriation of particles from conventional RFB.[15] The fate of single particles injected into the freeboard region was shown to depend on their size, large particles being returned to the particle bed and small particles being elutriated.[15] A further size separation of particles occurs in the cyclone. The functioning of the latter is based on the flow pattern in the chimney and cyclone, which continues to be rotating, as in the fluidization chamber.

Conclusions

The new concept of a rotating fluidized bed in a static geometry (RFB-SG)[16] is presented and experimentally investigated using one and the same nonoptimized fluidization chamber design with either large diameter, low density polymer particles or small diameter, higher density alumina particles, at different solids loadings, and in vertical and horizontal operation. The fluidization gas is injected tangentially in the fluidization chamber via multiple gas inlet slots in the outer cylindrical wall of the fluidization chamber, fluidizing the solids tangentially and inducing the rotating motion of the particle bed. As a result, the solids experience a radially outwards centrifugal force. A radially inwards gas-solid drag force is induced by positioning a chimney with one (in the present investigation) or multiple outlet slots centrally inside the fluidization chamber. As such, the gas is forced to move radially inwards, fluidizing the solids radially. The solids can be continuously fed and removed to and from the fluidization chamber via a solids inlet in one of the end plates of the fluidization chamber and a solids outlet in the other end plate of the fluidization chamber.

The gas flow being responsible for both the radial gas-solid drag force (Eqs. 1–6) and the rotational motion of the particle bed and the resulting centrifugal force (Eq. 8) in a similar way, allows to operate RFB-SG over a relatively broad gas flow rate range without too much altering the ratio of the centrifugal force and the gas-solid drag force.

Experiments are carried out in a 36 cm diameter, 13.5 cm long fluidization chamber with 12 tangential gas inlet slots and one chimney outlet. In all cases, a rotating fluidized bed and a reasonable to good gas-solid separation can be obtained, provided that the rotational speed is sufficiently high, that is the gas flow rate is sufficiently high. With a gas flow rate of about 0.2 m^3/s, bed rotational speeds between 3 and 7 rps and radial slip velocities of at least 2 m/s are obtained. The behavior of the rotating fluidized bed is, however, very different for the polymer and the alumina particles, in particular at higher solids loadings. Whereas the polymer particles tend to form a dense uniform bed, the alumina particles tend to form a less dense and less uniform bed. With the current nonoptimized fluidization chamber design, the radial fluidization is minimal with the polymer particles, but quite pronounced with the alumina particles. Bubble formation is observed with the alumina particles. Bubbles originating at the gas inlets are transported tangentially and radially or mainly tangentially, depending on the solids loading. Solids losses via the chimney are negligible with the polymer particles, but somewhat more pronounced with the alumina particles as a result of the radial expansion, the bubble formation, and some recirculation near the chimney immediately downstream of the chimney outlet. An optimization of the fluidization chamber design and the operating conditions is necessary for each given type of particles. The main parameters of the fluidization chamber design are the outer and inner (chimney) radius and the length of the fluidization chamber, the number of gas inlets to the fluidization chamber, the gas inlet design, the number of outlets to the chimney, and the solids feeding and removal system. With both types of particles, channeling and slugging and an uneven distribution of the gas over the gas inlets may occur at too low rotational speeds or too low solids loadings. Finally, preliminary attrition tests with the polymer particles show minimal losses of fines by attrition.

Acknowledgments

Luc Wautier at UCL is greatly acknowledged for the technical realization of the project, for his help with the experiments, and for the helpful discussions.

Prof. Guy Marin and Prof. Geraldine Heynderickx at the Ghent University (Belgium) and Prof. Jamal Chaouki at TPRF) are greatly acknowledged for their interest in this work and for the helpful discussions.

The mechanical engineering department at the Université catholique de Louvain (UCL) is greatly acknowledged for the use of the fast digital camera.

Sander Decock (ODK) is greatly acknowledged for the helpful discussions.

Notation

a = acceleration, m/s^2
d = diameter, m
F = flow rate, m^3/s
L = length of the fluidization chamber, m
P = gas phase pressure, Pa
r = radial position, m
R = outer radius of the fluidization chamber, m
$\underline{S}$ = surface area, m^2
$\underline{u}$ = gas phase velocity, m/s
$\underline{v}$ = solid phase velocity, m/s
V = volume of the fluidization chamber, m^3

Greek letters

β = drag coefficient, kg/m^3/s
ε = volume fraction, /
ϕ = sphericity factor, /
μ = viscosity, Pa s
ω = angular velocity, rad/s
ρ = density, kg/m^3

Subscripts

g = gas phase
p = particle
s = solid phase
r = radial
t = tangential

Literature Cited

1. Quevedo JA, Nakamura H, Shen Y, Dave RN, Pfeffer R. Fluidization of nanoparticles in a rotating fluidized bed. Presented at the *Proceedings of AIChE Annual meeting 2005*. Cincinnati, OH, 2005.
2. Ahmadzadeh A, Arastoopour H, Teymoour F. Rotating fluidized bed an efficient polymerization reactor. Presented at the *Proceedings of AIChE Annual meeting 2005*. Cincinnati, OH, 2005.

3. Qian G-H, Burdick IW, Pfeffer R, Shaw H, Stevens JG. Soot removal from diesel engine exhaust using a rotating fluidized bed filter. *Adv Environ Res*. 2004;8:387–395.
4. Watano S, Nakamura H, Hamada K, Wakamatsu Y, Tanabe Y, Dave RN, Pfeffer R. Fine particle coating by a novel rotating fluidized bed coater. *Powder Technol*. 2004;141:172–176.
5. Watano S, Imada Y, Hamada K, Wakamatsu Y, Tanabe Y, Dave RN, Pfeffer R. Microgranulation of fine powders by a novel rotating fluidized bed granulator. *Powder Technol*. 2003;131:250–255.
6. Quevedo J, Pfeffer R, Shen Y, Dave R, Nakamura H, Watano S. Fluidization of nanoagglomerates in a rotating fluidized bed. *AIChE J*. 2006;52:2401–2412.
7. Qian G-H, Bagyi I, Burdick IW, Pfeffer R, Shaw H, Stevens JG. Gas-solid fluidization in a centrifugal field. *AIChE J*. 2001;47:1022–1034.
8. Howley MA, Pfeffer R. The hydrodynamics of a rotating fluidized bed. Presented at the *Proceedings of AIChE Annual meeting 2005*. Cincinnati, OH, 2005.
9. Saunders JH. Particle entrainment from rotating fluidized beds. *Powder Technol*. 1986;47:211–217.
10. Qian G-H, Bágyi I, Pfeffer R, Shaw H, Stevens JG. A parametric study of a horizontal rotating fluidized bed using slotted and sintered metal cylindrical gas distributors. *Powder Technol*. 1998;100:190–199.
11. Qian G-H, Bágyi I, Pfeffer R, Shaw H, Stevens JG. Particle mixing in rotating fluidized beds: inferences about the fluidized state. *AIChE J*. 1999;45:1401–1410.
12. Kroger DG, Levy EK, Chen JC. Flow characteristics in packed and fluidized rotating beds. *Powder Technol*. 1979;24:9–18.
13. Chen Y-M. Fundamentals of a centrifugal fluidized bed. *AIChE J*. 1987;33:722–728.
14. Fan LT, Chang CC, Yu YS, Takahashi T, Tanaka Z. Incipient fluidization condition for a centrifugal fluidized bed. *AIChE J*. 1985;31:999–1009.
15. Chevray R, Chan YNI, Hill FB. Dynamics of bubbles and entrained particles in the rotating fluidized bed. *AIChE J*. 1980;26:390–398.
16. de Broqueville Axel. Catalytic polymerization process in a vertical rotating fluidized bed. Belgian Patent 2004/0186. Internat. Classif: B01J C08F B01F; Publication Number: 1015976A3.
17. Wen YC, Yu YH. Mechanics of fluidization. *Chem Eng Prog Symp Ser*. 1966;62:100–111.
18. Ergun S. Fluid Flow through Packed Columns. *Chem Eng Progr*. 1952;48:89.
19. De Wilde J. A rotating fluidized bed in a static geometry. *Prog Rep UCL* 2005;1:1–45.

Manuscript received Aug. 16, 2006, and revision received Jan. 15, 2007.